Proceedings World Geothermal Congress 2010
Bali, Indonesia, 25-29 April 2010

Magnetotelluric Experiments in the Aliaga Geothermal Field, Western Turkey

Cemal Kaya [*] and Ahmet Tugrul Basokur [**]

[*] Cumhuriyet Üniversitesi, Mühendislik Fakültesi, Jeofizik Müh. B, Kampüs 58140 Sivas, Turkey;

presently Kayen Enerji A.S., Koza Sokak No: 37/6, GOP, Ankara, Turkey

[**] Ankara Üniversitesi, Mühendislik Fakültesi, Jeofizik Müh. B, Tandoğan 06100 Ankara, Turkey

caubkaya@gmail.com; basokur@eng.ankara.edu.tr

Keywords: Magnetotellurics, Directional Noise, Smoothing, Two-dimensional Inversion.

ABSTRACT

Western Turkey has a number of hot-water springs and attracts attention for new prospects. For example, the geological investigations carried out around Aliaga shows that the region may have valuable resources for the geothermal energy production. Consequently, the magnetotelluric (MT) and transient electromagnetic (TEM) methods have been applied to delineate the source rock, faults and other subsurface features over a profile that consists of 21 measurement stations in this probable geothermal field. The length of the profile was 5 km.

Since the measurement profile is close to petrochemical and metallurgy manufacturing sites, the MT data have been severely distorted by directional industrial noise. The noise is typically "V" type around 10 Hz. After the rotation of the data to the principal axis of the impedance tensor, the level of noise contamination becomes relatively high in the mode perpendicular to the profile direction. A new smoothing algorithm is developed to overcome the directional noise problem. The method is based on the combination of a fitting function that simulates the behaviour of the frequency-normalised impedance. The random and systematic noises were represented by weight coefficients derived from the differences between the measured and smoothed frequency-normalised impedance data. The smoothed apparent resistivity datasets are then computed from the impedance data in order to employ as the input of the interpretation algorithms.

The static-shift correction has been employed by the help of theoretical MT datasets obtained from the one-dimensional earth models that are computed from the inversion of the transient electromagnetic method (TEM) data measured in the same location. The MT data have been interpreted by the application of two-dimensional inversion techniques. The computed resistivity-depth section has been interpreted in view of geology of the area. An overall picture of the subsurface including major faults has delineated and the promising parts of the geoelectrical section for geothermal energy are identified.

1. INTRODUCTION

The western part of Turkey consists of a number of promising geothermal fields as a consequence of young, volcanic activities that provide a magma heat source, porousness reservoir, impermeable cover and sufficient capability of the water cycle. Among many others, the Aliaga Geothermal Field, north of Izmir Bay, is notable because of its closeness to industrial regions. The Aliaga Geothermal Field has developed inside a large graben system of NW-SE strike and is located in the northwest of the Izmir–Ankara suture zone. Geochemical analysis of cold and hot waters indicates the possibility of a geothermal fluid of 200 ^{0} C. Previous geophysical surveys have led to the discovery of a weak geothermal source. Three boreholes shown in Figure 1 produced hot water of 15-20 lt/sec with temperature of 90-95 ^{0} C. The depths of the boreholes were 625, 1136 and 1146 meters, respectively. Since the explored source is not sufficient to satisfy the industrial demands, subsequent investigations were carried out using the magnetotelluric (MT) method, because of its relatively higher depth of investigation. The natural electrical and magnetic fields were measured at 21 stations over a straight line of 5 km. The central loop transient electromagnetic (TEM) was also used as a complementary induction method at all locations of MT measurements to apply static shift corrections.

2. GEOLOGY OF THE STUDY AREA

The geological information presented here is compiled and summarized from the works of Genc and Yilmaz (2000) and Esder et al. (1991). Figure 1 is the geological map of Aliaga and its vicinity, also indicating the location of MT stations. Izmir flysch of the Upper Cretaceous age constitutes the basement of the region. It consists of successive layering of schists and metasandstones. The metamorphic schist occurs in green schist facies conditions; it shows epiclastic characteristics and contains recrystallized limestone blocks. Soma Formation (Ts) was deposited over the basement, constituting discordance. This formation is in volcanogenic sediment characteristics, and it consists of thick layering of clayey limestone, marl, mudstone, sandstone, siltstone, fine limestone, tuffite sequences at the bottom and a variety of volcaniclastics at the upper levels (Esder et al., 1991). The average thickness of Soma Formation is estimated as 1800 m. The Aliaga volcanics overly Soma Formation with angular discordance.

During the Middle Miocene period, the region was, generally, shore, but sometimes covered by shallow waters. During this period, andesitic lavae and intercalated pyroclastics named as Aliaga pyroclastics (Tap) was deposited (Esder et al., 1991). The total thickness is about 350 m. Hatundere dacites (Tryl), Bozdivlit basaltic andesites (Tba) and Dumanlidag andesites (Tand) overlying the Middle Miocene period constitute Aliaga's pyroclastics. All of them are of sialic origin in calc-alcalic character and constitute the most important units of Aliaga's volcanics. Hatundere dacites first occurred in the Upper Miocene and covered a large area. An interruption occurred in the volcanism after the generation of Hatundere dacites and erosion started during this period. The current thickness of dacites varies between 75 and 300 m, while the initial thickness was 750 m before erosion. Quaternary consists of

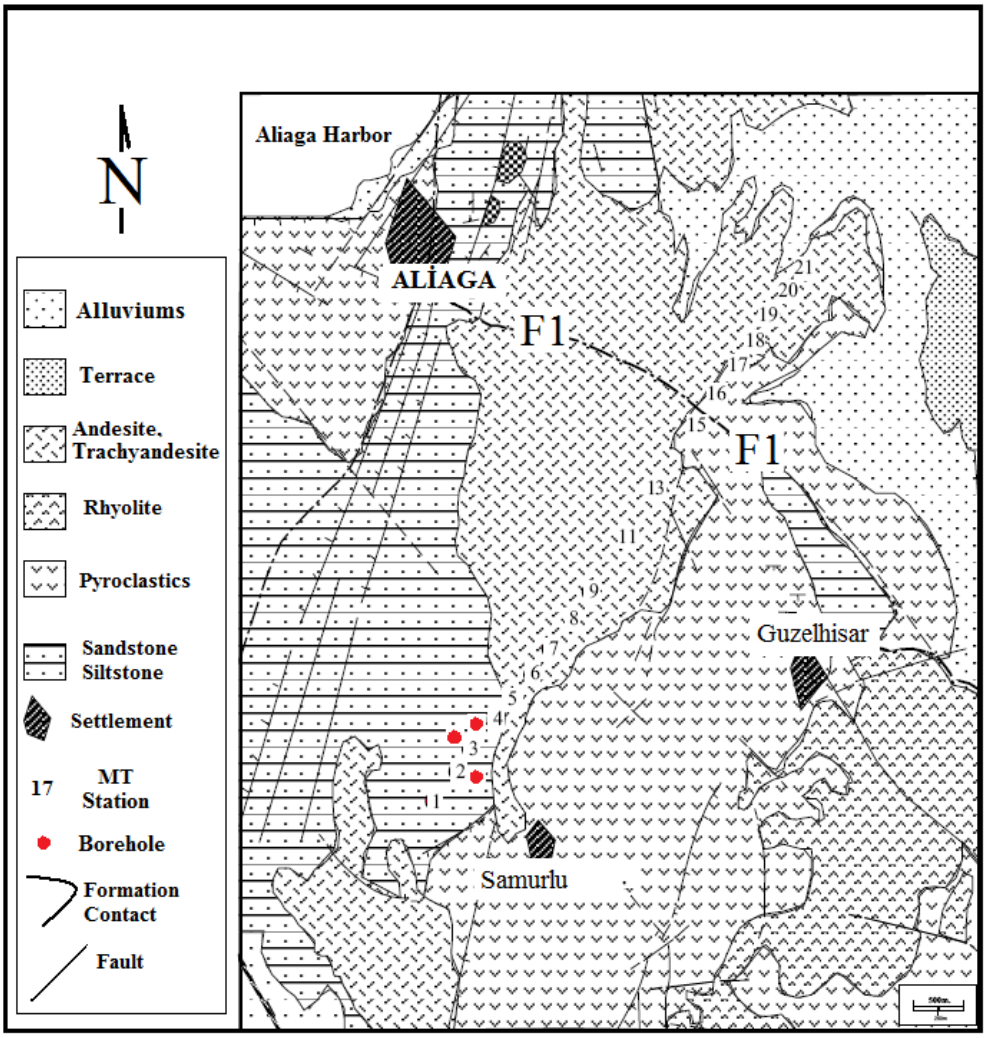

Figure 1: Geological map of Aliaga (Esder et al., 1991) and magnetotelluric measurement stations. The red dots indicate borehole locations.

alluvium and debris. There are some large, flat areas inside the valleys. The majority of alluvial units consist of gravel and blocks that are transported by streams (Esder et al., 1991).

3. STRUCTRAL GEOLOGY AND GEOTHERMAL MODEL

The tectonic evolution of the investigation area can be subdivided into paleotectonic and neotectonic periods. In the paleotectonic period, the folding, faulting and thrusting of autochthone and allochthon units are related to the northeastward subducting of the oceanic crust of the northern branch of Neothetis. The Paleotectonic period, and overall compression affecting the region, ended by the end of Eocene period. In the Neotectonic period, folding, faulting and rifting of the region were controlled by the westward movement of the Anatolian block, caused by the northward pushing of the Arabian Plate. The timing and characters of volcanism was controlled by the north-south directed extension that was the main reason of the volcanic activity in the region in this period. The trends in the Neotectonic period can be classified into three groups, as follows:

1) NE-SW tectonic trends (Middle Miocene-Upper Miocene),
2) NW-SE tectonic trends (Lower Miocene-Quaternary),
3) WNW-ESE tectonic trends (Lower Miocene-Quaternary).

NW-SE tectonic trends are related with the current graben progress and have a relatively young morphology. The earthquakes associated with the graben development occur through the zones in the NW-SE direction. The seismic intensity is in accordance with the Dumanlidag volcanic centre. The focal depths of the earthquakes are, generally, in the range of 6.5-20 km. These active faults allow the transportation of geothermal fluids towards the surface.

A conceptual geothermal model was constructed by incorporating all geological information complied in the regional scale, as shown in Figure 2. This model postulates that the meteoric water joins the geothermal system in the east and southeast part of the region and is warmed by the heating source beneath the Dumanlidag volcanic centre. It is also possible that some additional fossil magma chambers still exist. The hot water spreads into the system by circulating, firstly, towards the surface through fault zones, and later horizontally. The hot water is accumulated in the permeable zones of Izmir flysch and Soma Formation. Finally, it is discharged as hot water in the Bicer and Ilicaburun springs. The movement of geothermal fluids is from southeast to northwest.

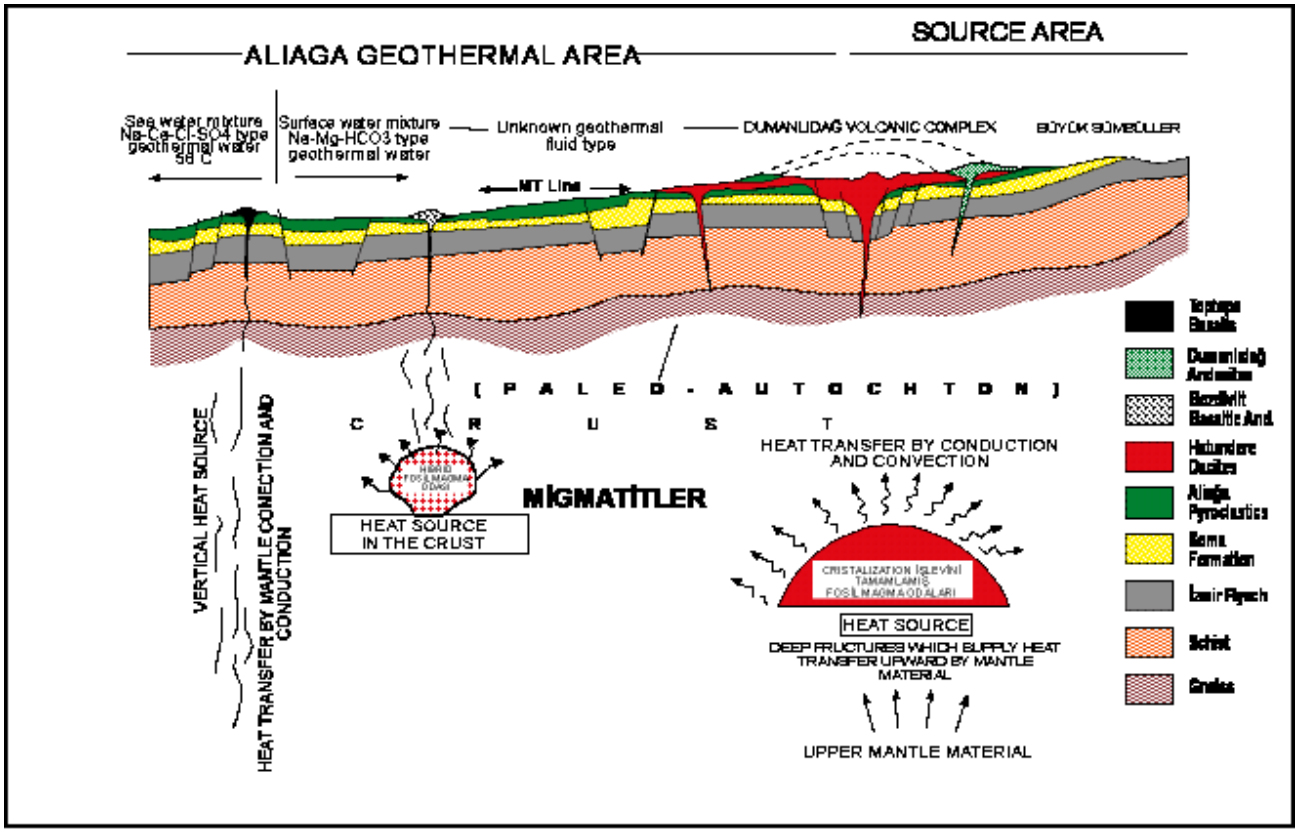

Figure 2: Conceptual geothermal system for Aliaga field (Esder et al., 1991).

4. FIELD SURVEY

The investigation area is located in the neighbourhood of the Dumanlidag volcanic centre. The location of MT line in the conceptual model is illustrated in Figure 2. The fieldwork was completed in September 1999. The seven-channel Phoenix-V5 equipment was used for the measurements of two orthogonal electric and three orthogonal magnetic (H) field components (E_x, E_y, H_x, H_y, H_z) at 21 stations. The distance between the stations was approximately 250 m constructing a profile of 5 kms in length. Additionally, two orthogonal magnetic field components (RH_x, RH_y) were measured at a remote station that was fixed at a distant location. Non-polarizable lead-lead chloride electrodes were used because of their long-term stability (Petiau and Dupis, 1980). The horizontal and vertical components of the magnetic field were measured with induction coils and an air loop on the ground respectively. The high- and low-frequency bands included frequency ranges of 320-7.5 and 6-0.00055 Hz, respectively. We acquired the MT data in the lower band for longer than 24 hours. The impedance values in 40 frequencies were computed after the Fourier transformation of time-domain data by using cascade decimation. The TEM-57 model transmitter and PROTEM receiver, both manufactured by Geonics, were used for the data acquisition of the TEM data in the time range of from 0.0881 to 7 milliseconds.

5. DATA PROCESSING

The elements of the 2x2 impedance (Z) tensor are derived from the complex ratios of the orthogonal components of the horizontal electric and magnetic fields in the frequency domain. Since all the measurement stations are located over a line in our case, the data only permit the application of a two-dimensional interpretation process that requires the identification of TE and TM modes corresponding to electric and magnetic fields parallel to the geologic strike respectively. Since the geological strikes are not known in advance, the components of electromagnetic fields are measured in geomagnetic (or arbitrary) directions and the impedance tensor is rotated to principal axes. The strike direction often changes with depth in field practice and, accordingly, the rotational angle varies at each frequency. For two-dimensional structures, there are many conditions and consequently many possible schemes to determine the rotational angle (Simpson and Bahr, 2005). Here, we minimized the diagonal elements of the impedance tensor. There are two possible strike directions for a certain frequency and the interpreter identifies the TE and TM modes by using geological and geophysical information (Vozoff, 1991). Figure 3 shows an example of the rotational apparent resistivity and phase data, together with the rotation angles. The MT data have been contaminated by the directional noise around 10 Hz because of the petrochemical and/or metallurgical factories close to the investigation area. The directional noise is dominant (or existing) only in one of the modes. A special smoothing method was then applied to the rotated data, in order to reduce the directional noise contamination, but it was impossible to reduce the noise in three stations and, accordingly, only 18 stations were selected for the interpretation.

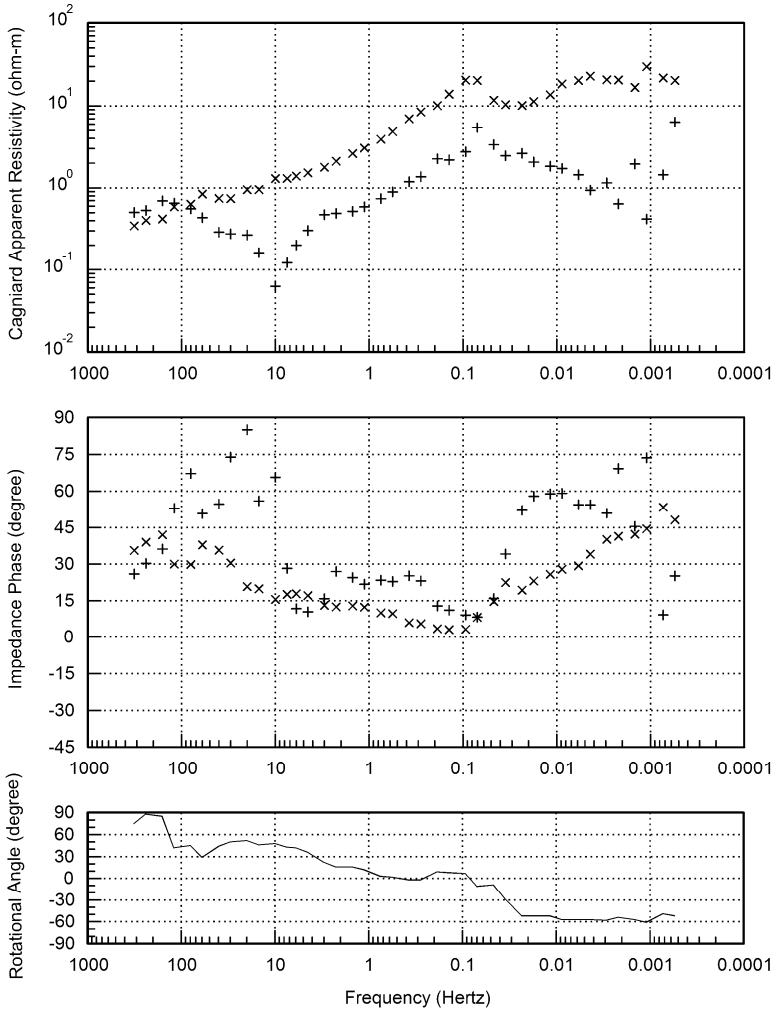

Figure 3: Rotated data at the measurement station of MT-01. From top to bottom: Cagniard's(1953) apparent resistivity, impedance phase and rotation angles. (x) and (+) indicates xy-component and yx-component, respectively.

Two types of noise sources result from the measurement conditions. These are 'random' and 'systematic' errors (Bevington, 1969). Random errors are the fluctuations in observations estimated for a certain frequency. A measure of the fluctuation, for example, standard deviation, can be derived from the statistical analysis. Then, a weight coefficient inversely proportional to the standard deviation or other types of weight related to the confidence range of the measured data can be assigned to each frequency. However, the directional noise is a kind of systematic error and, consequently, statistical analysis is not useful in expressing uncertainties because, although multiple data estimation for a certain frequency can provide a datum value with high precision, it will not provide a good approximation of the accurate value. Thus, the technique adopted here to overcome the systematic errors, including the directional noise, is based on the searching for a fit between the measured MT curve and its smoother counterpart, constructed by a combination of simple fitting functions distributed along the horizontal frequency axis. Similar methods have been used in DC electrical methods for different purposes (Santini and Zambrano, 1981; Santini and Zambrano, 1983; Niwas and Israil, 1986). The method used here is adapted from Basokur et al. (1997) and Basokur(1999). The method was utilized by using the frequency-normalized impedance (FNI) function defined by Basokur(1994) as the measured data:

$$Y_{xy} = \frac{Z_{xy}}{(i\omega\mu)^{1/2}} = \frac{1}{(i\omega\mu)^{1/2}} \frac{E_x}{H_y} \qquad (1)$$

where ω is the angular frequency and μ is the magnetic permeability of free space. *Z* is known as the impedance and is determined from the ratio of the electric field to the magnetic field.

The smoothing operation involves the approximation of the measured data by a linear combination of a simple fitting function:

$$Y^*(f_i) = w_i . \sum_{j=1}^{m} b_j \, g(f_i; \varepsilon_j) \quad i=1, 2,\ldots,n \qquad (2)$$

where $Y^*(f)$ is an approximation of the measured *Y(f)* function and is determined to within a desired precision. *m* and *n* is the number of fitting function and the number of sample values of the FNI function, respectively. ε_j coefficients determine the position of each function along the horizontal frequency axis and are fixed depending on the frequency range and the number of fitting functions. w_i is the weight coefficients corresponding *j*th frequency. The unknown b_j decomposition coefficients are determined by minimizing the differences between the measured and smoothed data (Basokur et al., 1997):

$$\boldsymbol{b} = (\boldsymbol{G}^T\boldsymbol{G})^{-1} \,.\, \boldsymbol{G}^T\boldsymbol{y} \qquad (3)$$

where $\boldsymbol{b}$ is the *mx1* matrix whose elements are the unknown decomposition coefficients (b_j). $\boldsymbol{G}$ is the *nxm* matrix whose elements consist of the fitting functions that are distributed along the frequency axis. $\boldsymbol{y}$ is a *nx1* matrix that contains the measured data. Since the weight coefficients (w_i) are also unknown, the equation (3) is solved twice. All weights are set to equal to unity in the first pass of the algorithm. Before the second pass of the algorithm, a new set of weight coefficients is computed by using the differences between the measured and approximated data obtained in the first pass (Basokur, 1999):

$$w_i = \exp\left\{-\left[Y(f_i) - Y^*(f_i)\right]^2 / \alpha\right\} \qquad (4)$$

where α is the shape factor and is calculated as follow:

$$\alpha = \frac{2}{n}\sum_{i=1}^{n}\left|Y(f_i) - Y^*(f_i)\right| \qquad (5)$$

and inserts the information about the overall noise contamination of the whole data into the calculation of a weight coefficient belonging to a certain frequency. The above expressions will yield weight values distributed between zero and unity. The large discrepancies between a measured and an approximated value will lead to weight values that are relatively very small thus giving less degree of importance to the outlier data values. Once the decomposition coefficients are determined by the equations (3) and (4) then the approximated values of $Y^*(f)$ can be constructed by the linear combination of the fitting functions using the known decomposition coefficients at any desired abscissa points by using the equation (2).

The computation scheme applied here differs from the conventional smoothing operation. By allowing a variable misfit, the interpreter can freely decrease or increase the number of fitting functions in an interactive way in order to find an acceptable approximated FNI curve. If the number of fitting functions is decreased, then a smoother curve than the previous one is obtained. The method suggested here uses the superiority of the trained human eye to be the best tool for the identification of an acceptable, approximated curve from among many possible solutions. The algorithm also permits the re-sampling of the data, which can be implemented by constructing a new set of approximated data at equally spaced frequency values in the logarithmic axis. Figure 4 shows an example of the smoothing process that the 'V'-type directional noise becomes unnoticeable. The data are re-sampled in the frequency range of 100 – 0.001 Hz and are represented by 41 values, such that eight sample values per decade of logarithmic axis. After the smoothing operation, the static-shift correction was applied to apparent resistivity data to reduce the effect of small or large scale lateral resistivity variations before generating pseudo-sections. The central loop TEM was applied as a complementary induction method at all locations of MT measurements for this purpose. A one-dimensional model is derived for a certain station from the inversion of TEM data. The theoretical MT data are calculated for this one-dimensional earth model. The measured MT curves in both TE and TM modes are then shifted upward or downward along vertical axis towards the theoretical MT data in order to employ the static-shift correction. The MT data aquired over a line are traditionally presented as pseudo-section. Figures 5 and 6 illustrate the corrected apparent resistivity together with the phase data in TE and TM modes, respectively. The general overview of the pseudosections suggests a three-layered earth model and a normal fault located approximately between 3.6 and 3.8 km of the measurement line.

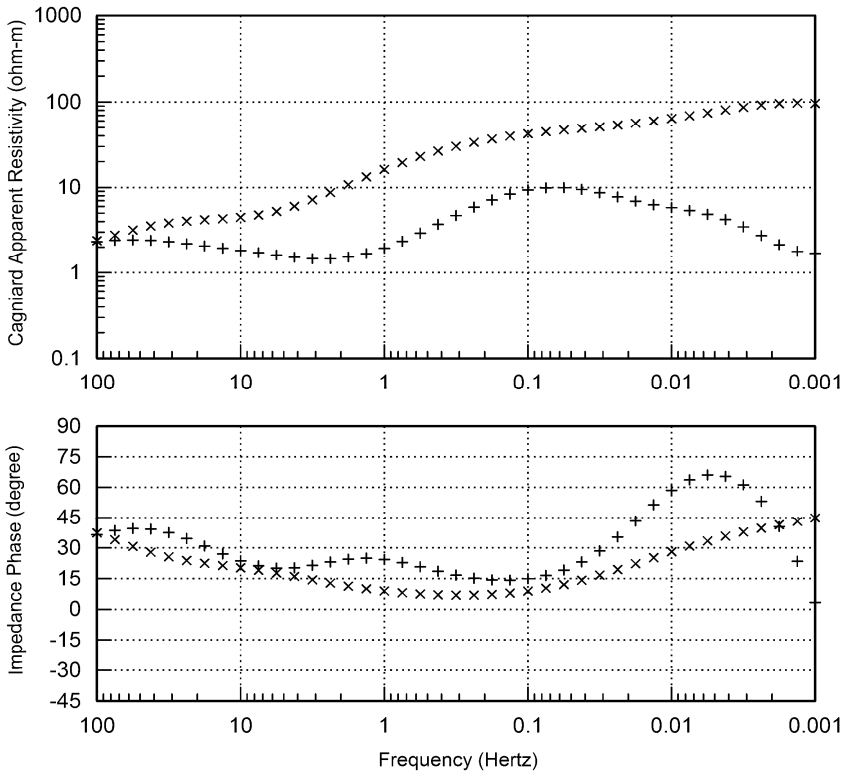

Figure 4: Smoothed Cagniard's(1953) apparent resistivity and phase data at the measurement station of MT-01. The static-shift correction is applied to the apparent resistivity data. (x) and (+) indicates xy-component and yx-components, respectively.

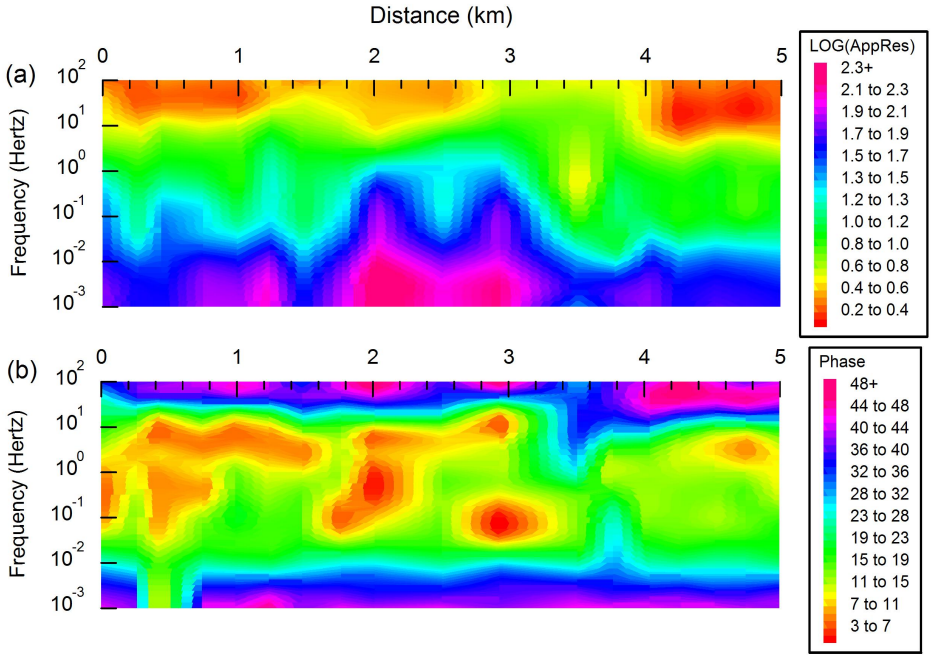

Figure 5: Cagniard's(1953) apparent resistivity and phase data (TE mode).

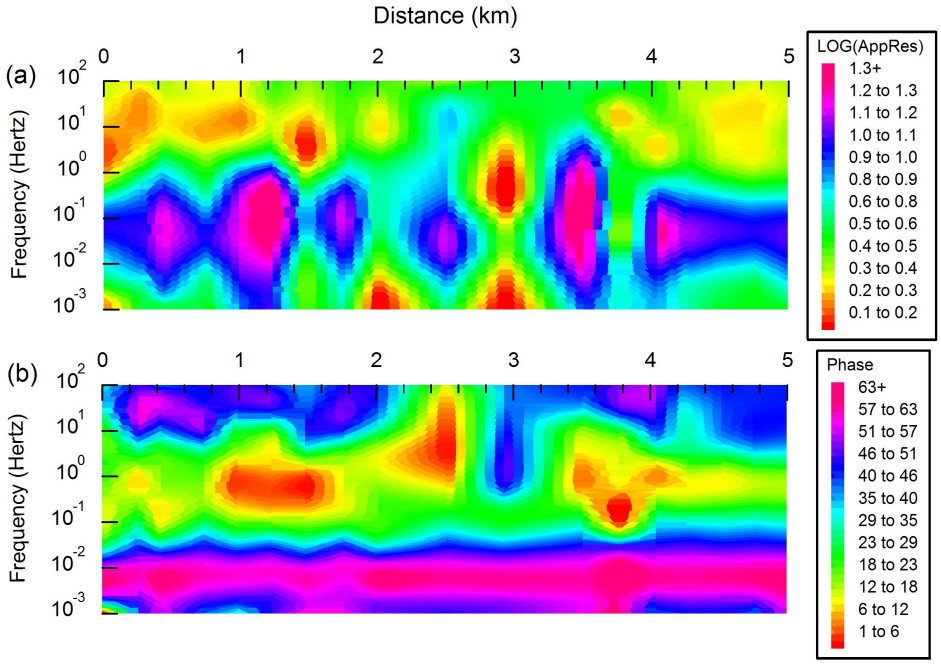

Figure 6: Cagniard's(1953) apparent resistivity and phase data (TM mode).

6. RESULTS OF TWO-DIMENSIONAL INVERSION

The purpose of the conventional two-dimensional (2D) magnetotelluric imaging is to obtain a distribution of the intrinsic resistivity in the subsurface. The extraction of the geological information from the produced resistivity image is performed by the human interpreter. A piece of commercial software (WingGlink®) was used for the computation of the resistivity image. Firstly, the 2D forward modelling mesh is constructed by subdividing the subsurface into a large number of small cells. The theoretical MT data corresponding to the 2D model are computed by the application of the finite-difference method. The initial model is updated until a satisfactory fit is obtained between the measured data and model response. In this way, the intrinsic resistivity values of each cell are solved by the application of the conjugate gradient inversion technique. In order to derive a geologically interpretable resistivity image, the variation in resistivity values of neighbouring cells is interconnected so that the neighbouring cells affect the solution of the resistivity value of the central cell to some degree. We have used the smoothed and re-sampled apparent resistivity data in the inversion process because of the directional noise. The phase data are not included in the inversion, because the noise contamination of the phase data was extremely high before the smoothing operation. Consequently, the smoothed phase data are not particularly reliable.

The superficial part of the 2D-resistivity image and its geological interpretation are illustrated in Figure 7. The boundary between the metamorphic basement and overlying sedimentary unit (Soma Formation) is delineated very well. The depth of basement increases towards the end of the profile. It is somewhat difficult to identify the Soma Formation from the overlying volcanic units. Three faults, named as F1, F2 and F3, are interpreted by making use of the resistivity discontinuities in the image section. The F1 fault is considered a normal fault that reaches the upper crust, as shown in Figure 7, which represents the deeper part of the resistivity image. The depth of the interface between the upper and lower crusts is approximately 12 km.

7. CONCLUSION

The interpretation of the MT line 5 km in length around Aliaga gives a rough picture of the geological situation. The survey line is close to an industrial zone containing metallurgical and petrochemical factories. For this reason, the data are contaminated by the directional noise at around 10 Hz. This noise is somewhat removed by a special smoothing algorithm that uses a combination of some basis functions. The smoothing does not increase reliability of the data, but it makes the inversion software run in a stable way. The depth values in the interpretation section have some uncertainties for two reasons. Firstly, many models providing a reasonable fit between theoretical and measured datasets may exist. Hence the degree of noise contamination of the data is an important factor influencing the parameter estimation. Secondly, the 2D inversion tends to give a blurred image of the subsurface. The outcome is usually a smooth picture of the actual structures, and we may expect that one interpreted geological unit can be confined within a much narrower zone (or vice-versa) and still explain the data as long as the vertically integrated conductivity is kept unchanged. However, excepting the exact depth values of interfaces, a gross feature of the subsurface is well outlined by the MT method. This is sufficient for deciding the promising parts of the resistivity image section for the geothermal exploration purposes. The interpreted 2D model given in Figure 7 is also supported by the previous boreholes that indicated the hot water potential of Soma formation. Since the hot water is accumulated in the permeable zones, we suggest some drill holes between MT-06 and MT-09 and also between MT-15 and MT-17 in view of the slope of Soma formation and the location of interpreted faults that both indicate probable geothermal targets.

ACKNOWLEDGMENTS

We gratefully acknowledge the Mineral Research and Exploration Institute of Turkey (MTA) for providing equipment and funding for the data acquisition. The hardware and software for the computation and interpretation are provided by the Scientific and Technical Research Council of Turkey (TUBITAK), under grant number YDABÇAG-198Y091, and Ankara University, under grant number 2000.07.05.021.

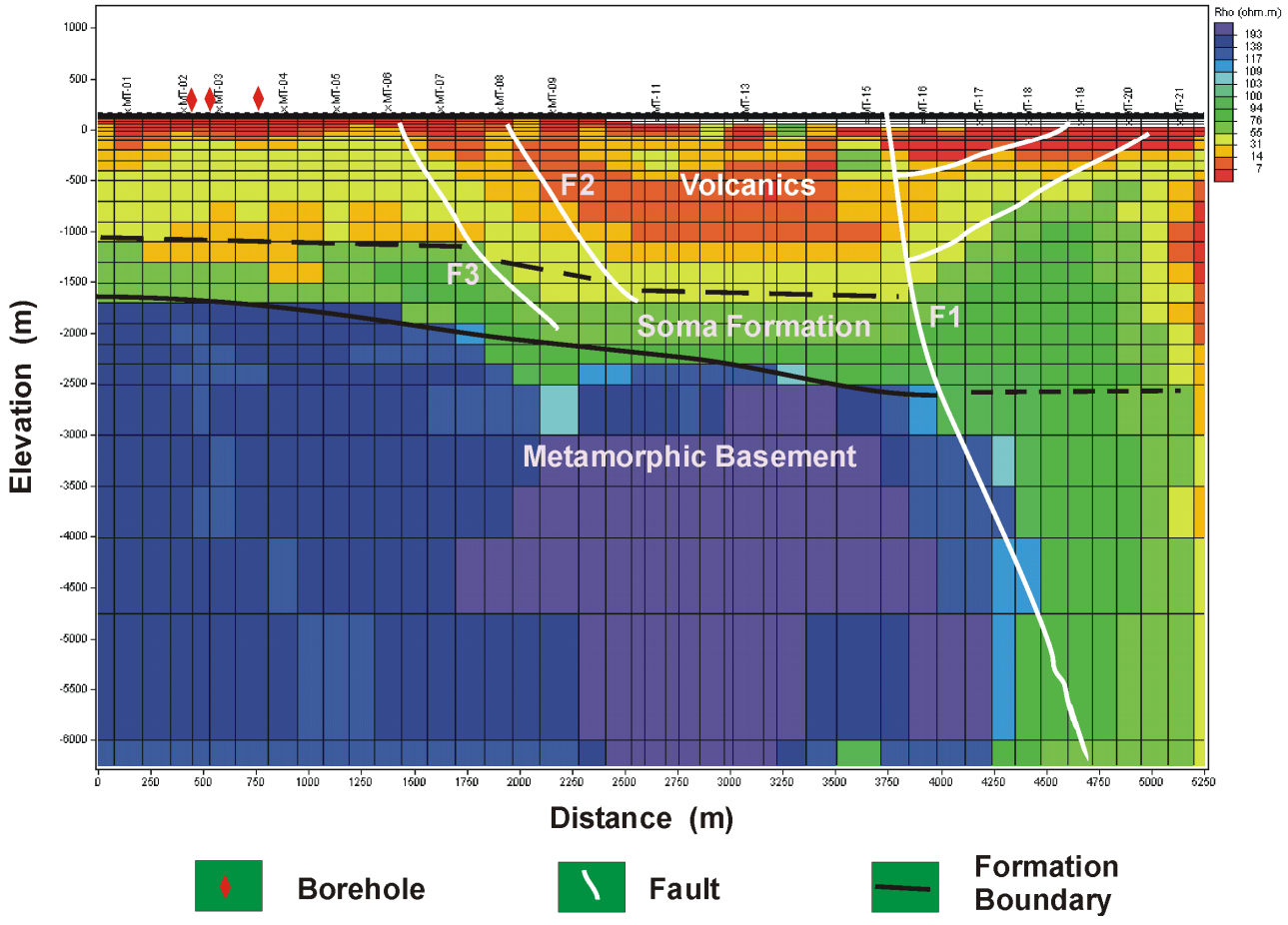

Figure 7: Two-dimensional resistivity image obtained from the MT data and its geological interpretation.

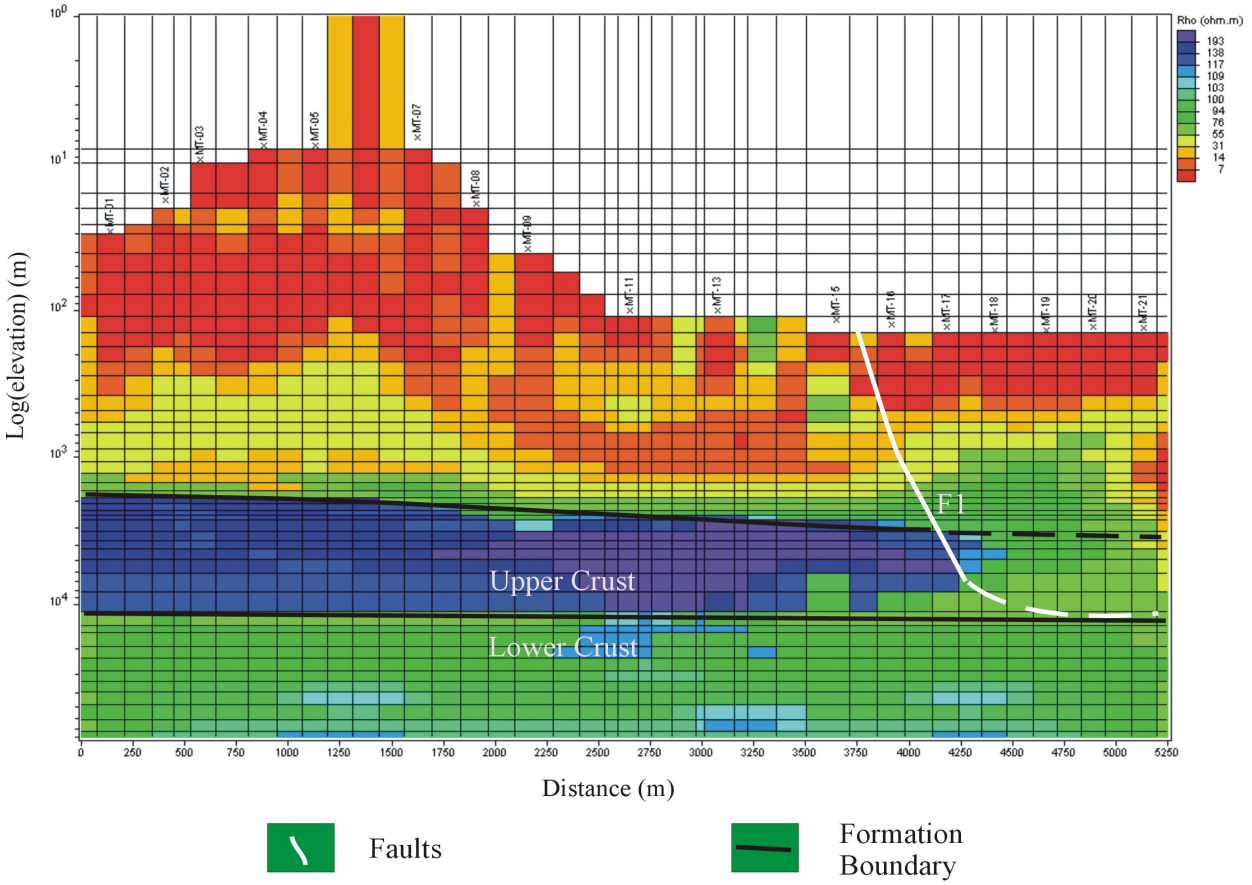

Figure 8: Deeper part of the resistivity section showing the normal fault F1 and depths of upper- and lower-crust interfaces.

REFERENCES

Basokur, A. T.: Automated 1-D Interpretation of Resistivity Soundings by Simultaneous Use of the Direct and Iterative Methods, *Geophysical Prospecting*, **47**, (1999), 149-177.

Basokur, A. T.: Definitions of Apparent Resistivity for the Presentation of Magnetotelluric Sounding Data, *Geophysical Prospecting*, **42**, (1994), 141-149.

Basokur A.T., Kaya, C., and Ulugergerli, E. U.: Direct Interpretation of Magnetotelluric Sounding Data Based on the Frequency-normalized Impedance Function, *Geophysical Prospecting*, **45**, (1997), 21-37.

Bevington P.R.: Data Reduction and Error Analysis for the Physical Sciences, (1969), McGraw–Hill Book Co.

Cagniard, L.: Basic Theory of the Magnetotelluric Method of Geophysical Prospecting, *Geophysics*, **18**, (1953), 605-635.

Esder, T., Yakabag, A., Sarikaya, H., and Cicekli, K.: Geology and Geothermal Potential of Aliaga (Izmir) Region (in Turkish), Mineral Research and Exploration Institute of Turkey (MTA) Report No: 9467, (1991).

Genc, S. C., and Yilmaz, Y.: Geology of Vicinity of Aliaga and its Neotectonics, Proceedings of Symposium of Seismicity of West Anatolia, Izmir, Turkey, (2000), 152-159.

Niwas S., and Israil, M.: Computation of Apparent Resistivities Using an Exponential Approximation of Kernel Functions, *Geophysics*, **51**, (1986), 1594-1602.

Petiau, G., and Dupis, A.: Noise, Temperature Coefficient, and Long Time Stability of Electrodes for Telluric Observations, *Geophysical Prospecting*, **28**, (1980), 792-804.

Santini, R., and Zambrano, R.: A Numerical Method of Calculating the Kernel Function from Schlumberger Apparent Resistivity Data, *Geophysical Prospecting* **29**, (1981), 108–127.

Santini, R., and Zambrano, R.: A Generalized Method to Calculate Standard Curves for Geoelectrical Soundings, *Geoexploration*, **21**, (1983), 93-103.

Simpson, F., and Bahr, K.: Practical Magnetotellurics, Cambridge University Press, (2005), ISBN 0 521 81727 7, 254 pp.

Vozoff, K.: The Magnetotelluric Method in "Electromagnetic Methods in Applied Geophysics, Volume 2, Application Parts A and B" (Edited by M. N. Nabighian), (1991), Society of Exploration Geophysicists.